Hindawi
Geofluids
Volume 2022, Article ID 8471638, 13 pages
https://doi.org/10.1155/2022/8471638

Research Article

Research on the Characteristics of Coal Bump and Monitoring and Early Warning in Hujiahe Coal Mine

Fei Yu,[1] **Tong Zhang**,[2,3] **and Zhen Wei**[1,3]

[1]*School of Mining Engineering, Anhui University of Science and Technology, Huainan, 232001 Anhui, China*
[2]*Institute of Energy, Hefei Comprehensive National Science Center, Anhui, Hefei 230031, China*
[3]*State Key Laboratory of Mining Response and Disaster Prevention and Control in Deep Coal Mines, Anhui University of Science and Technology, Huainan, 232001 Anhui, China*

Correspondence should be addressed to Tong Zhang; 1099731996@qq.com

Received 25 January 2022; Revised 1 June 2022; Accepted 22 June 2022; Published 8 August 2022

Academic Editor: Gangwei Fan

Under the high intensity mining disturbance, coal bump is easily triggered by the sudden release of large amount of elastic energy contained in the coal body, which seriously affects coal mine safety production. Triaxial experiments were used to study the damage characteristics of coal samples subjected to loading at the 401103 working face of Hujiahe coal mine, and the critical value of peak strength of coal samples was investigated. Based on the characteristics of the mechanical damage behavior of coal samples obtained from the triaxial experiment, the statistics of the occurrence of coal bump events at the 401103 working face were conducted through numerical simulation and field monitoring to study the areas that need to be focused on prevention and control, with a view to providing basic research for deep coal mining. The results show the following: (1) the strength of coal samples is "weakened" by stress loading, and the fracture penetrates the coal body interface leading to the formation of tensile-shear damage of coal samples. The value of the damage variable for the coal sample in the initial damage stage is 0; at the damage stabilization stage, the values of damage variables were derived to be located at 0.03~0.14. The bearing capacity of the coal sample decreases rapidly during the accelerated development period. (2) According to the simulation and field monitoring, it is known that 0~100 m in front of the coal mining face belongs to the key monitoring area. (3) With the advancement of the working face, different coal pillar widths have obvious effects on the vertical stress, and stress increase and decrease zones appear on both sides of the coal column, and the peak stress shows the characteristics of increasing first and then decreasing with the advancement of the working face. The width of the working face has a great influence on the change of vertical stress. When the sensitivity of the vertical stress to the width of the working face increases, the stress concentration phenomenon will occur, and a large amount of elastic energy gathered in the coal body is suddenly released to induce coal bump.

1. Introduction

With the rapid development of China's economy, energy demand has increased dramatically; in situ multistress environment, a large amount of elastic energy is contained in the coal body; and to a certain extent, the sudden release of elastic energy aggravates the destruction of the coal body, which leads to the instability of the coal-rock system-induced coal bump events that gradually increased. Therefore, it is important to study the mechanical damage mechanism of coal damage and the prevention of key coal bump areas through numerical simulation and field monitoring. Coal bump, characterized by the dynamic vibration and rock-mass spallation, is directly correlated to the geological structure, in situ stress, and lithology. Due to the nonlinearity and mortal threat of the coal bump, numerous efforts and research interest have been focused on the mechanism and trigger factors [1–6].

For the complex nonlinear and dynamic mechanic properties, coal bump is regarded as a discontinuous problem, and a comprehensive method, including theoretical derivation, field measurement, and numerical simulation, was employed [7, 8]. The mining geometry and surrounding rock mass properties influence the concentration and

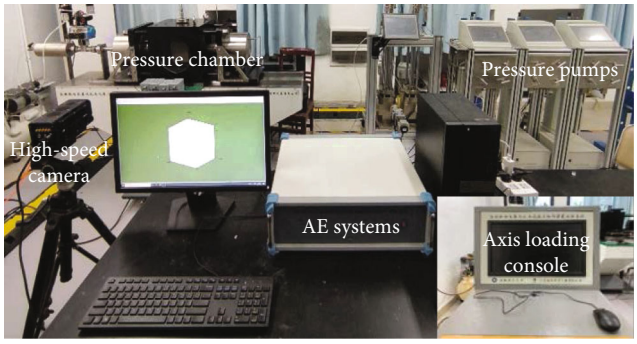

Figure 1: Three-axis dynamic and static loading experimental system.

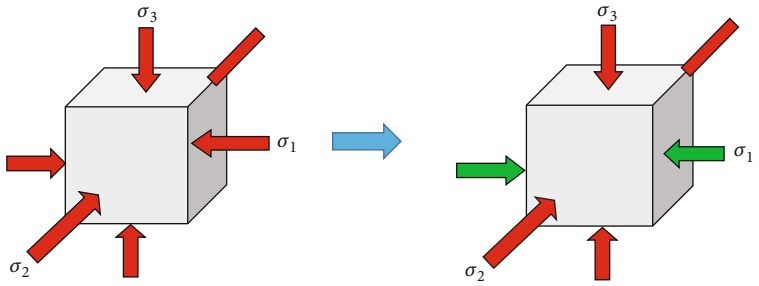

Figure 2: Loading and unloading 3D schematic (path 1).

instability of the elastic energy [9, 10]. The theoretical and numerical models, including "strength theory," "stiffness theory," and "energy theory" which are named "rock burst basic theory," were developed for the coal bump judgment and prediction [11]. Considering the influence of the geology and geomechanics, Thom [12] and Henley [13] developed a catastrophe theory for the prediction of the coal bump. Regarding the roof and the coal pillar as a testing machine and coal specimen system, Pan and Zhang [14] established a cusp catastrophe model. Using the catastrophe theory, Qin et al. [15] and Xu et al. [16] studied the instability mechanisms of the coal-pillar-and-roof system.

The static stress, seismic activity, or acoustic emission (AE) is the source of rock bursts and support damage [17]. Monitoring method, including EME, AE, electric charge, and microseismic (MS) monitoring as well as seismic velocity tomography, is the most popular method for monitoring and predicting the coal bump. Assuming the rock burst is caused by static and dynamic load superposition, He et al. [4] proposed the microseismic and electromagnetic coupling method for coal bump assessment. According to Lu and Dou [18], the relationship between the vertical stress gradient, seismic, and EME signals at the Sanhejian mine was investigated and a positive correlation was found between the number of seismic events, the vertical stress concentration factor, and the strength of the EME signal and the borehole [19]; it was concluded that microseismic monitoring systems were widely installed in deep mine, and the model calibration process, considering AE or microseismic source location and source parameter, was a challenge.

Most of the above studies on the characteristics of damage mechanical behavior of coal samples and the law of acoustic

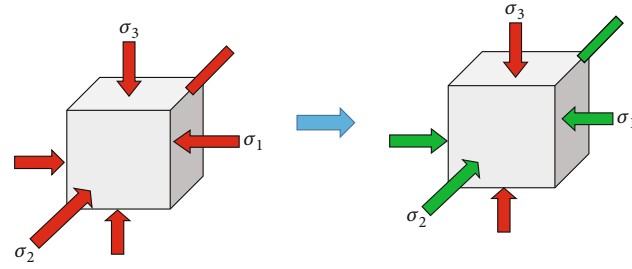

Figure 3: Loading and unloading 3D schematic (path 2).

emission signals are based on theoretical studies or numerical simulations, which have a single research means and deviations in the research results under the inversion of real geological conditions, and the determination of coal rock dynamic hazards and impact propensity is a macroscopic study based on field monitoring, and there are fewer studies on the damage mechanical characteristics of coal samples under different unloading stress paths in the true triaxial. To address the above problems, this paper designs experiments on the damage characteristics of coal samples under three different unloading stress paths using the true triaxial experimental system with Hujiahe coal mine engineering geology as the research background and investigates the peak damage strength of coal samples. Based on the experimental study, numerical simulation and field monitoring methods were used to analyze the key monitoring areas where coal bump occurred in Hujiahe coal mine and the effects of dynamic and static loading stress on the sensitivity of coal pillars and working face width.

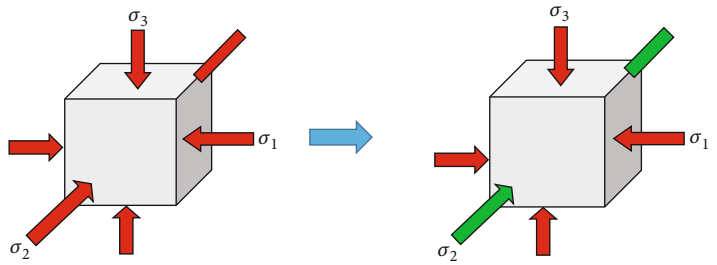

Figure 4: Loading and unloading 3D schematic (path 3).

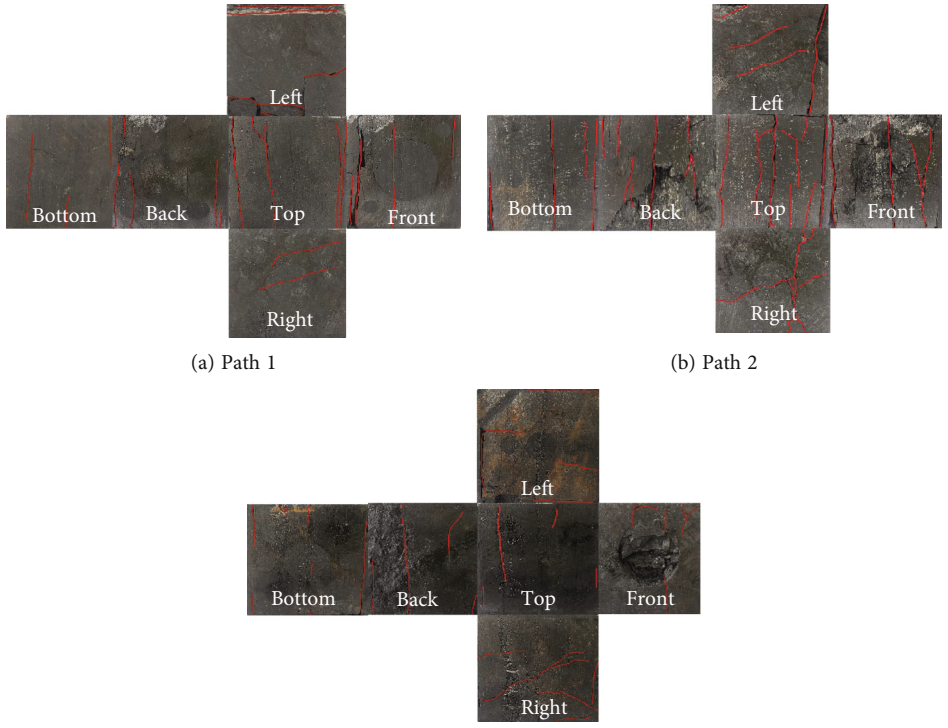

(a) Path 1

(b) Path 2

(c) Path 3

Figure 5: Deformation and damage characteristics of coal bodies in different paths.

2. Triaxial Experiment

2.1. Experimental Equipment. To study the mechanical damage behaviour, acoustic emission characteristics and coal bump mechanism of coal samples, the experiment uses the "three-axis dynamic and static loading experimental system." The experimental device can realize independent loading of three directions. The system consists of an acoustic emission monitoring system, a high-speed camera, an axial loading console, a pressure chamber, and a pressure pump, as shown in Figure 1.

2.2. Experimental Steps. Three excavation scenarios are often used in the mining process of Hujiahe coal mine: one is excavation along one side of the coal body, another is excavation along two symmetrical faces of the coal body, and another is excavation along two adjacent faces of the coal body. Therefore, the three stress paths in this paper correspond to the above three scenarios, respectively. In the three-dimensional diagram, $\sigma_1(X)$ indicates the minimum principal strain; $\sigma_2(Y)$ indicates the maximum principal strain; $\sigma_3(Z)$ indicates the intermediate principal strain; the red arrow indicates the loading direction, and the green arrow indicates the unloading direction.

Path 1: from Figure 2, first load the stress in three directions to the initial balance. Subsequently, the $\sigma_3(Z)$ direction was loaded. The $\sigma_1(X)$ direction was unloaded to 0 MPa after stabilization for 2 minutes.

Path 2: from Figure 3, first load the stress in three directions to the initial balance. Subsequently, the $\sigma_3(Z)$ direction was loaded. After stabilizing for 2 minutes, $\sigma_1(X)$ and $\sigma_2(Y)$ are simultaneously unloaded to 0 MPa.

Path 3: from Figure 4, first load the stress in three directions to the initial balance. Subsequently, the $\sigma_3(Z)$ direction was loaded. After stabilizing for 2 minutes, the $\sigma_2(X)$ direction was unloaded to 0 MPa.

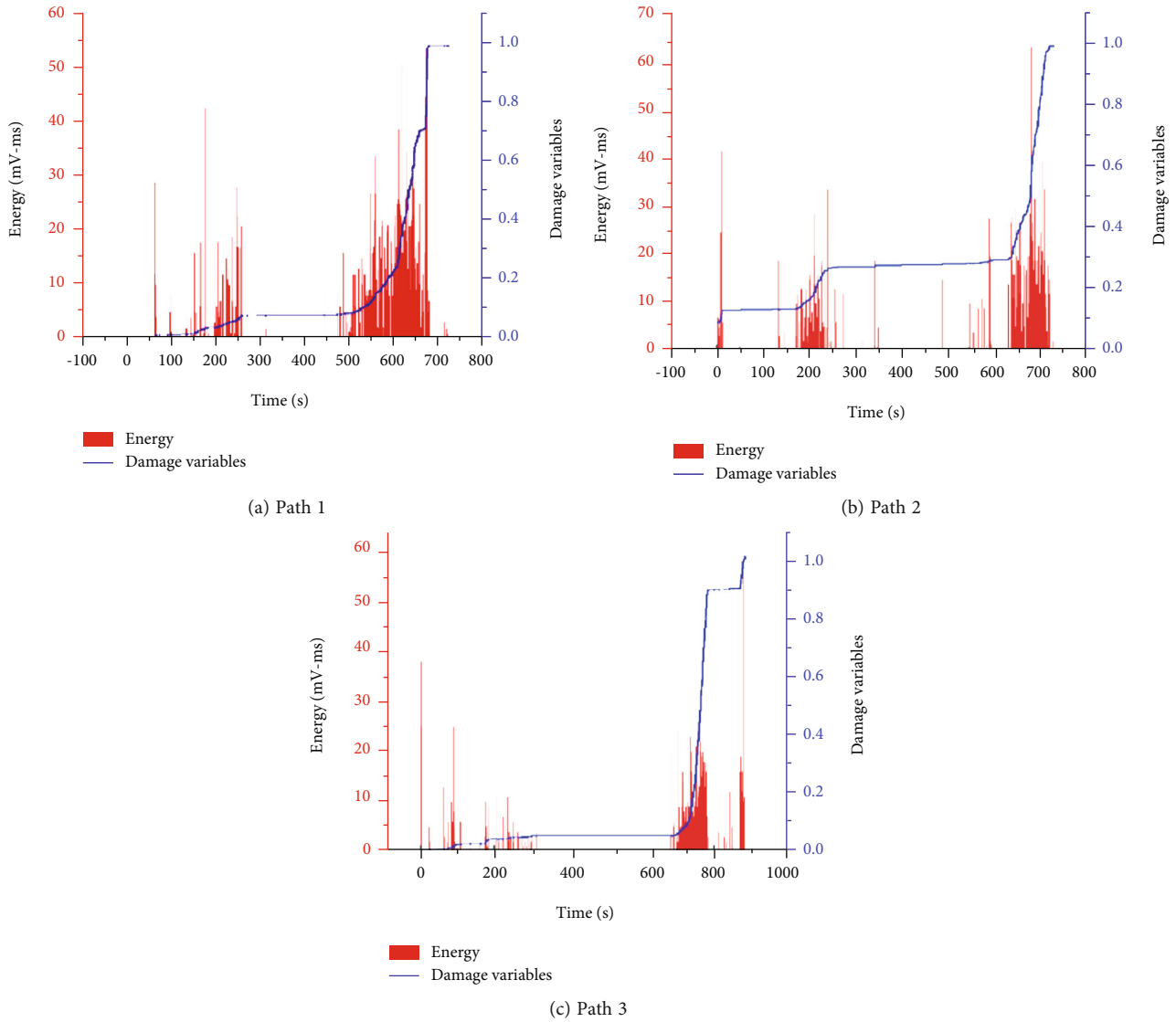

Figure 6: Diagram of AE energy and damage variables of coal body loaded under different stress paths.

2.3. Analysis of Experimental Results

2.3.1. Analysis of Damage Characteristics of Coal Samples. Analysis of coal body damage characteristics by 3 different stress paths was conducted.

In path 1, there are two macroscopic cracks on each of the front and back surfaces, less density of cracks on the left and right surfaces, and four macroscopic cracks on the top surface, as shown in Figure5(a).

In path 2, the fracture density of the front and back surfaces is larger relative to the fracture density of the path 1 test, with a total of 12 macroscopic fractures through the specimen, a smaller fracture density on the left surface, an annular fracture on the right surface, and a total of 12 macroscopic fractures through the specimen on the top and bottom surfaces as well as misalignment friction of coal powder particles inside the specimen, with the specimen in tensile-shear damage, as in Figure 5(b).

In path 3, stress concentration occurs on the front surface and three macroscopic fractures through the back surface, two macroscopic fracture on the right surface, fewer cracks on the top and bottom surfaces, as shown in Figure 5(c).

2.3.2. Acoustic Emission Response Characteristics. From Figure 6, it is concluded that in the three different stress paths, looking at the whole process of coal sample damage by loading, when the coal sample has a large rupture produced, the acoustic emission will show a sudden increase [20, 21]. In path 2, the increase of acoustic emission energy is not necessarily continuous but may also be jumping, which indicates that the energy release presents a scattered distribution when unloading two directions, and the stress is carried by two directions separately; the final energy release in each direction is smaller; in path 1 and path 3, the increase of acoustic emission energy basically presents as intensive and continuous, which indicates that the

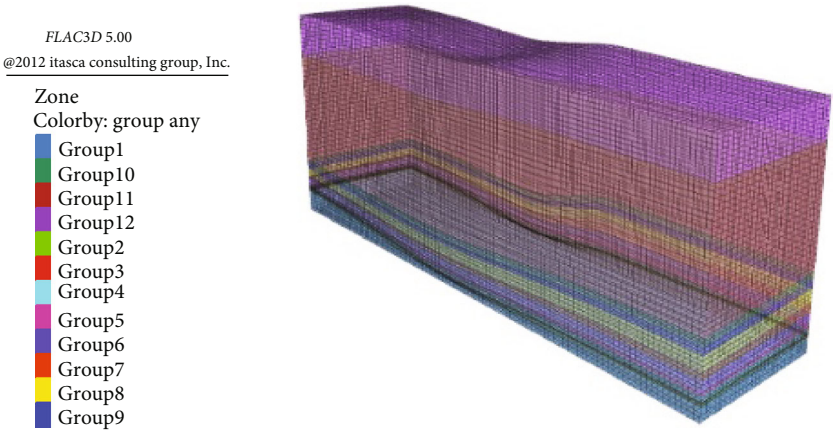

Figure 7: Modeling of the geology.

Table 1: Geometry and mechanical parameters of coal and rock.

Rock properties	Thickness (m)	Modulus of elasticity (GPa)	Poisson ratio	Cohesive strength (MPa)	Internal friction angle (°)	Tensile strength (MPa)
Sand shale	60	6.10	0.12	4.5	27	1.76
Sandstone	60	6.36	0.14	3.23	25	3.90
Mud stone	60	1.86	0.13	5.67	32	1.54
Fine sandstone	12	6.34	0.11	6.21	29	2.79
Silt stone	5	2.32	0.10	5.13	25	1.92
Coal	23	0.81	0.02	5.43	20	2.13
Silt stone	100	2.46	0.11	2.45	31	1.63

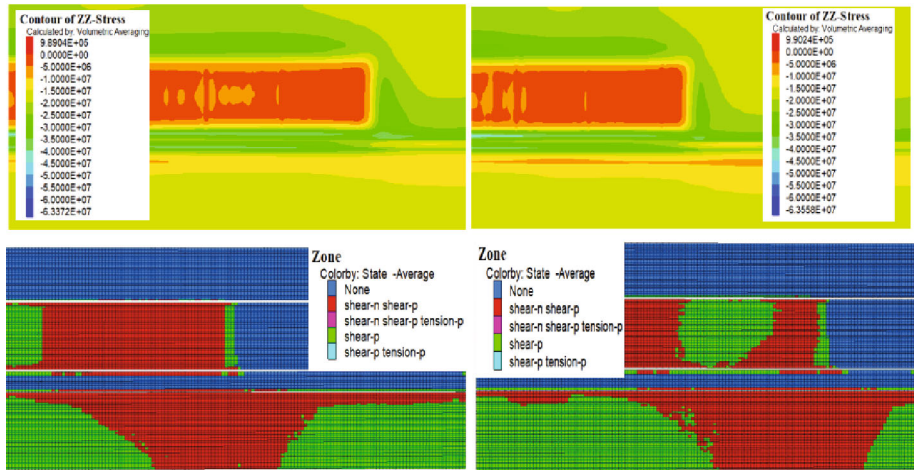

Figure 8: Evolution characteristics of the static stress and rock damage.

stress is borne by only one direction when unloading one direction; the final energy release is larger.

Damage to the coal body has gone through roughly 3 stages as follows.

During the initial damage stage, there is internal pore compressing of the coal sample in the initial stress and no fracture expansion; the internal structure of the coal sample is in a stable state; thus, the value of damage variable in the initial damage stage is 0.

In the damage stabilization stage, the pore space inside the coal sample changes to form tiny fissures due to the continuous loading of stress, and the fissures in the coal sample gradually stabilize and develop under the action of stress, with damage variable values reaching 0.03~0.14.

During the accelerated development stage, the value of the damage variable increases in 90° increments. As the fractures develop rapidly and extend throughout the coal sample during stress loading, the load bearing capacity of the sample

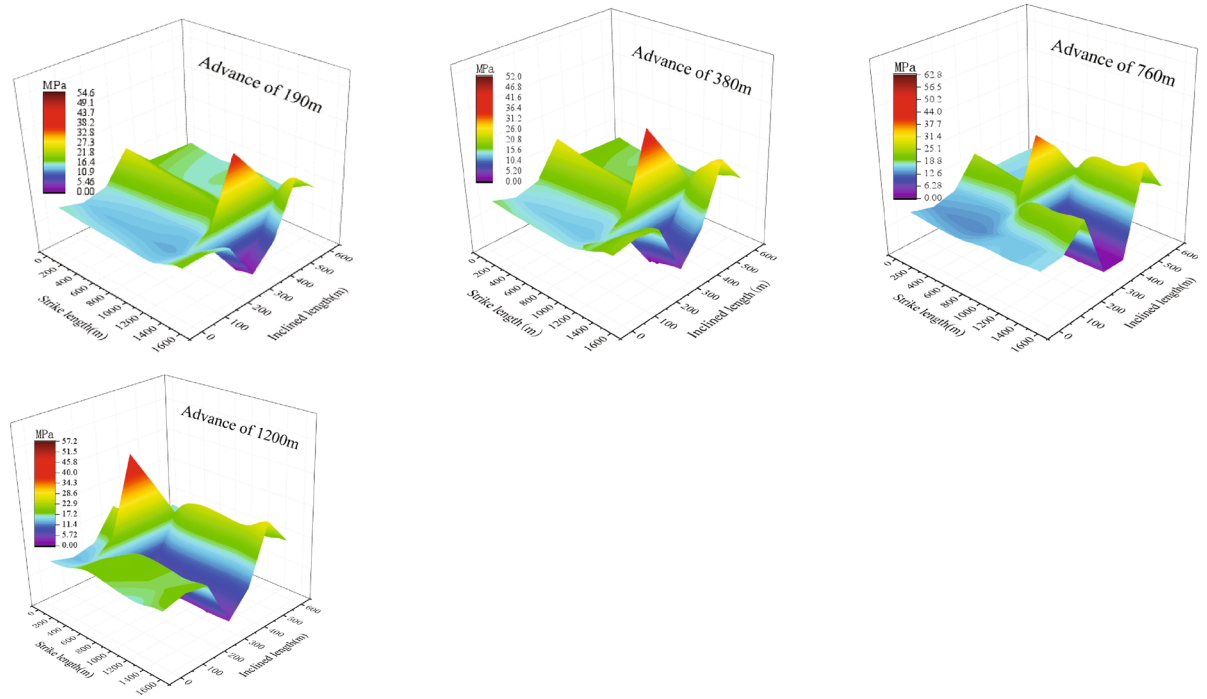

(a)

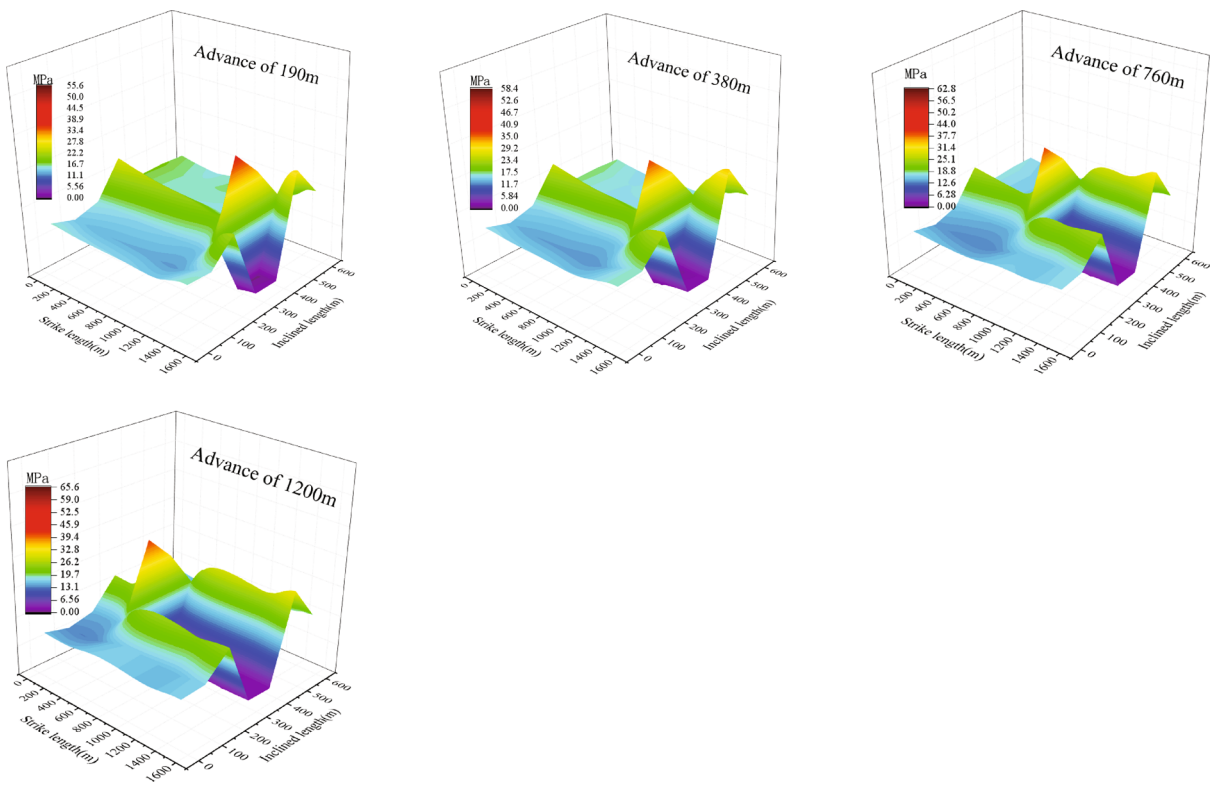

(b)

Figure 9: Continued.

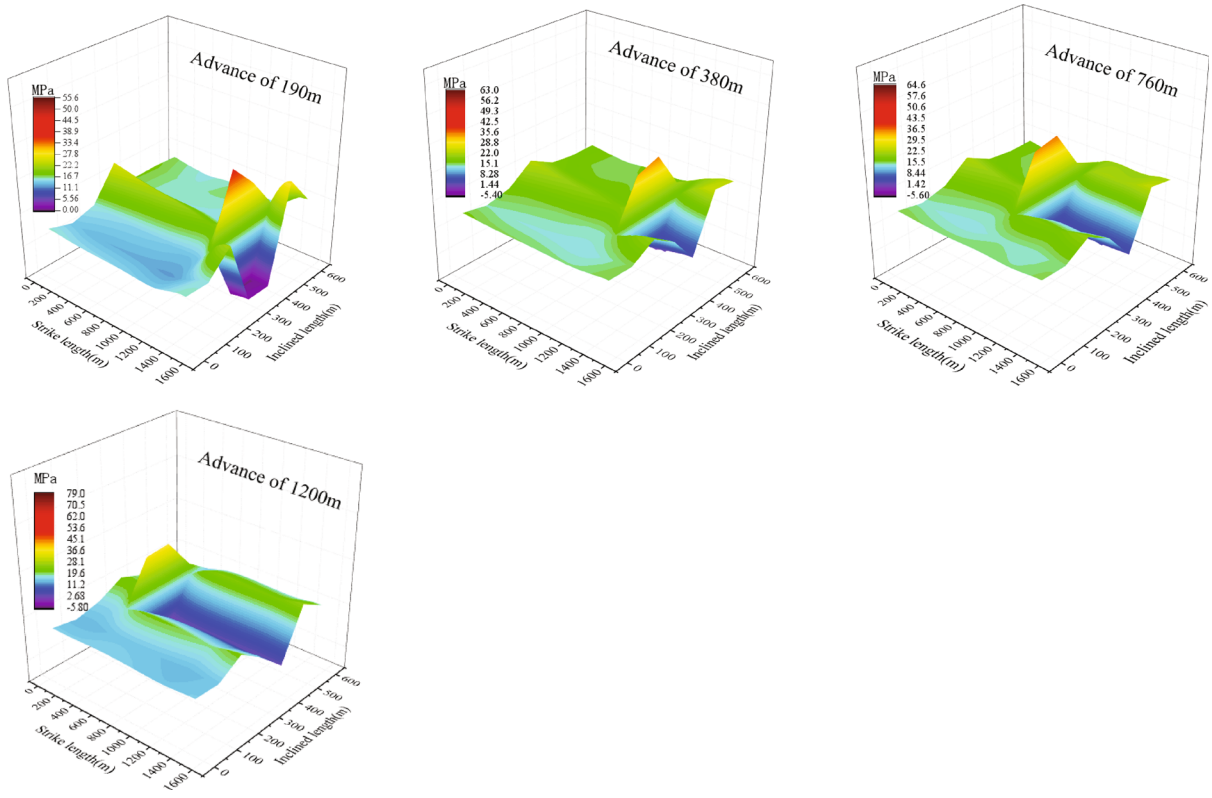

(c)

Figure 9: Vertical stress evolution for different pillar widths: (a) 5 m, (b) 25 m, and (c) 70 m.

weakens, the damage variable increases sharply, and the sample is completely destroyed.

3. Modeling of the Panel #401103

3.1. Geological Model. Hujiahe coal mine is located in Changwu County District, Xianyang City, Shaanxi Province, China, and is a typical coal bump coal mine. In order to accurately probe the area to be focused on in engineering applications, numerical simulation should be performed to restore the geological structure of coal#4. Coal #4 is the main coal seam with an average depth of 680 m, inclination of 5°, and thickness of 23 m.

In order to accurately describe the change of surrounding rock stress field and fracture field under the influence of mine activity, the simulation was conducted. In detail, a real geological model with a dimension of 1449 m × 606 m × 753 m (length × width × high) was established based on the lithology boreholes. The boundaries were constrained with a free roof, as shown in Figure 7. The geometry and mechanical parameters employed in the model are shown in Table 1.

3.2. Characteristic and Evolution of Static Stress of Surrounding Rock Mass. In order to accurately probe the area to be focused on in engineering applications, the mining process of the 401103 working face was first numerically simulated, as shown in Figure 8.Within 190~1200 m in front of the mining face, due to the large deformation of the roadway and effect of shear force, the stress is concentrated and the coal bump may occur. The region behind the mining face was damaged by shear and stretch under the effect of concentrated stress. The coal pillar-side stress concentration significantly increased with the advance of the mining face. The evolution characteristics of stress field and fracture field of the panel #401103 indicate that stress concentrations occur at the coal pillars and the gob in the range of 0~100 m in front of the working face, and there is a higher risk of coal bump in the roadway near the 401102 working face.

3.3. Effect of Coal Pillar Width. The coal mining was conducted under the condition of 5 m, 25 m, and 70 m coal pillar in mining geology. Figure 9 indicates that the vertical stress was characterized with increase and decrease in cloud picture, with the advance of the working face. The maximum vertical stress of the working face was 39.8 MPa and 35.8 MPa, respectively, for the coal pillar of 5 m and 25 m. For coal pillar of 70 m, the peak value of the mining face was 33.8 MPa to 35.1 MPa. As a result, the vertical stress decreased with the increase of the coal pillar width.

After coal mining, the stress concentration zone was presented ahead of the mining face, and the release stress zone was located in the gob. From Figure 10, it can be concluded that during the advance of the working face from 190 m to 760 m, the sensitivity of vertical stress to pillar width increases; when the working face advances 1200 m, the sensitivity of vertical stress to pillar width decreases.

With the advance of the working face, different coal pillar widths have a significant effect on the vertical stress and both

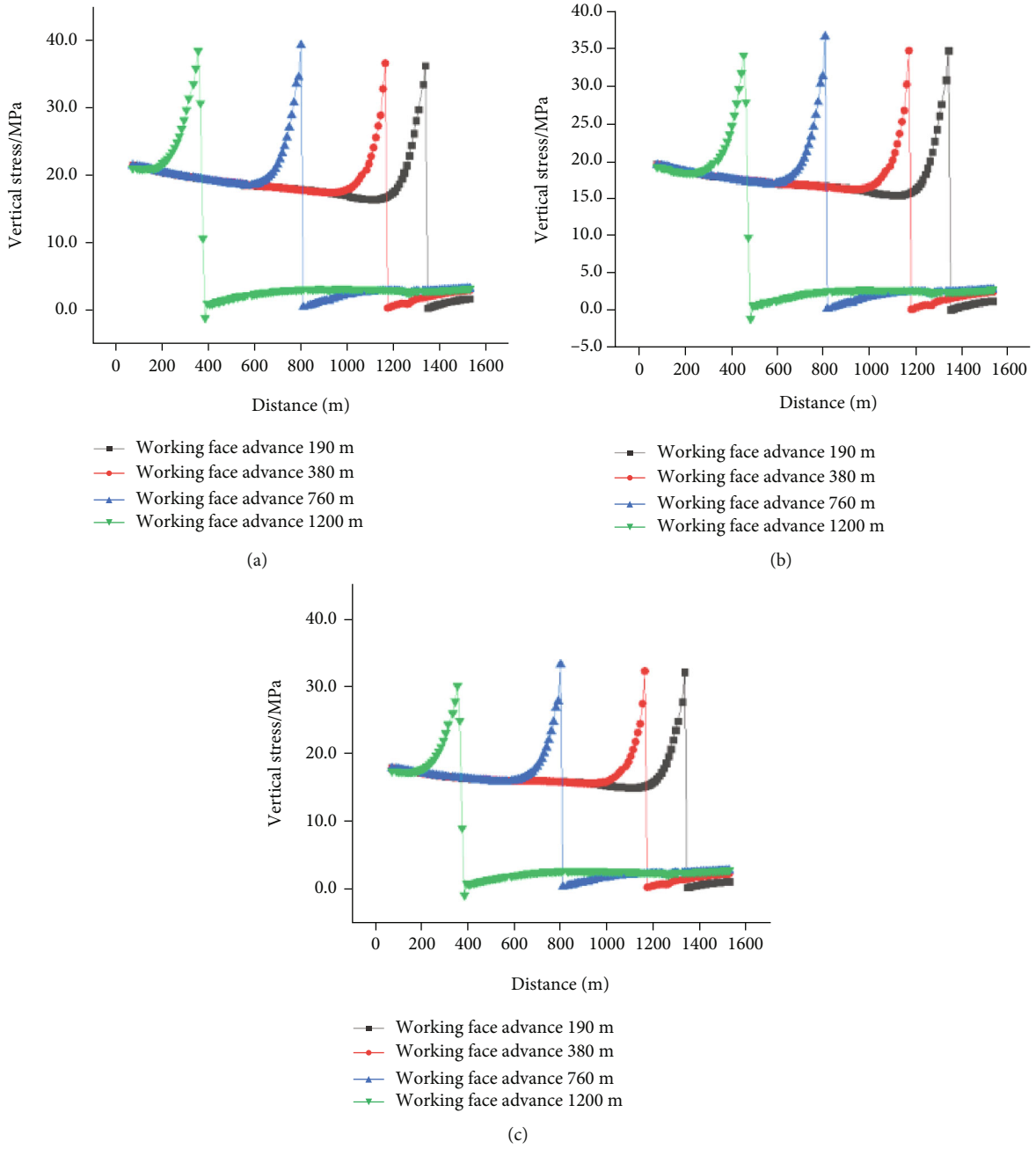

Figure 10: Vertical stress change in different pillar widths: (a) 5 m; (b) 25 m; (c) 70 m.

sides of the pillar show stress increase and decrease zones, and the peak stress shows that it increases first and then decreases with the advance of the working face. Finally, with the increase of the width of coal pillar from 5 m to 70 m, the peak of the vertical stress maintained stable and the morphology presented parallel distribution, as shown in Figure 10.

Figure 10 illustrates that the working face is advanced from 190 m to 760 m, the vertical stress shows a rising trend, and the stability was obtained after 760 m. The curve of stress peak was opposite to that of the pillar width in trend, with the increase of the pillar width from 5 m to 70 m and with the peak value decreasing from 39 MPa to 32 MPa.

3.4. Effect of Mining Face Width. In Figure 11, for the 250 m width of the working face, the vertical stress reached 39 MPa as the working face was advanced to 1200 m. The vertical stress reached 40 MPa as the mining face was advanced to 760 m. The vertical stress reaches 38 MPa and 37 MPa as the mining face was advanced to 380 m and 190 m. By contrast, for the 300 m width of the mining face, the vertical stress reaches 44 MPa as the mining face was advanced to 1200 m. The vertical stress reached 45 MPa as the mining face was advanced to 760 m. The vertical stress reached 39 MPa and 38 MPa as the mining face was advanced to 380 m and 190 m. Meanwhile, at the 350 m width of the mining face, the vertical stress reached

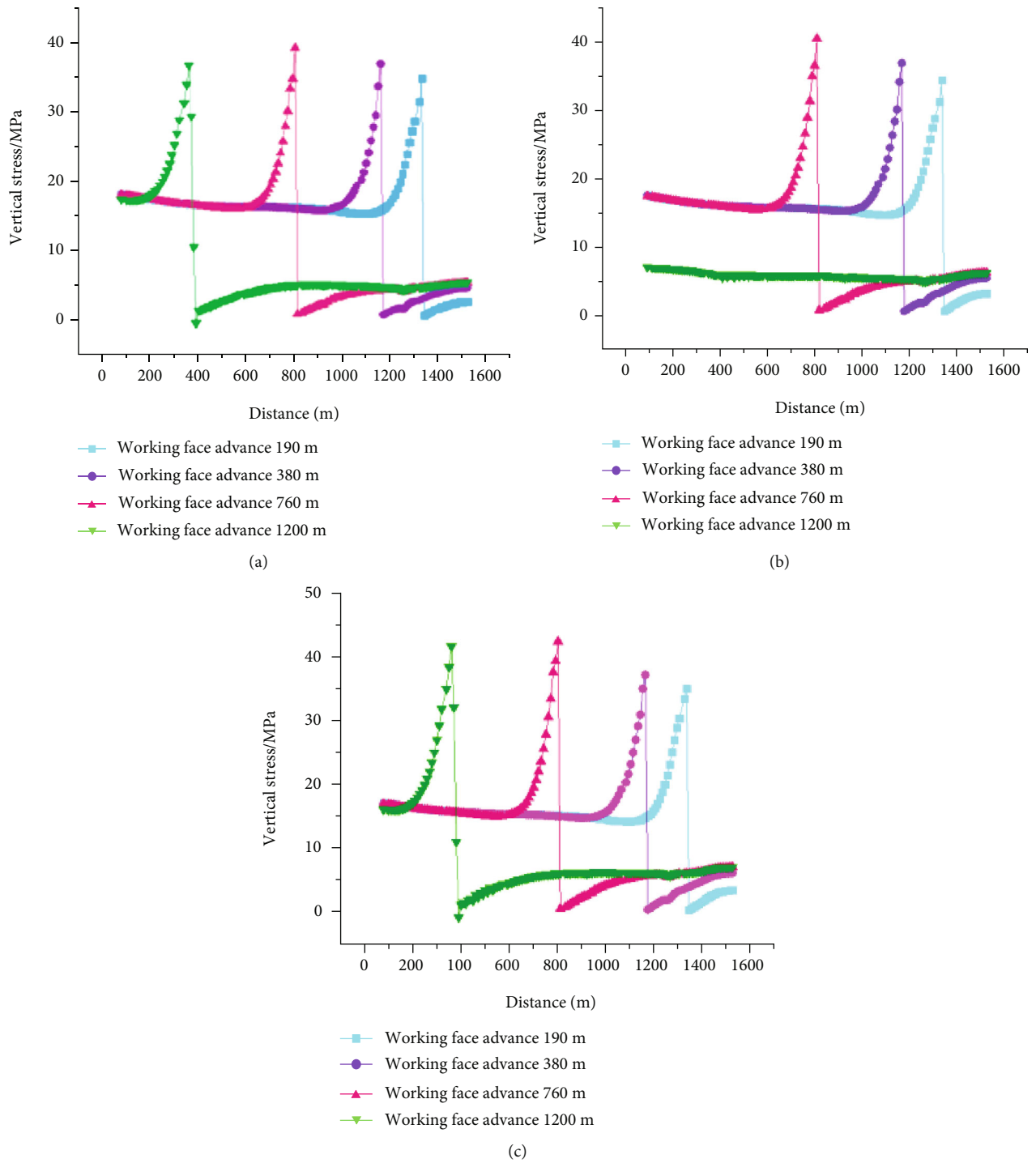

Figure 11: Vertical stress change in different working face widths: (a) 250 m, (b) 300 m, and (c) 350 m.

15 MPa as the working face advanced 1200 m. The vertical stress reached 42 MPa as the mining face was advanced to 760 m. The vertical stress reached 39 MPa and 38 MPa as the working face was advanced to 380 m and 190 m, respectively.

In Figure 11, with the advance of the working face, the stress increase zone and the reduction zone appeared on both sides of the coal pillar. The width of the working face has a significant effect on the vertical stress evolution. When the sensitivity of vertical stress to working face width increases, stress concentration phenomenon occurs, and the sudden release of a large amount of elastic energy accumulated in the coal body will lead to coal bump.

4. Coal Bump Theory Analysis

4.1. Coal Bump Theory Analysis. In Figure 12, a model of coal bump occurring at the coal pillar and working face caused by dynamic and static coupled stresses has been established based

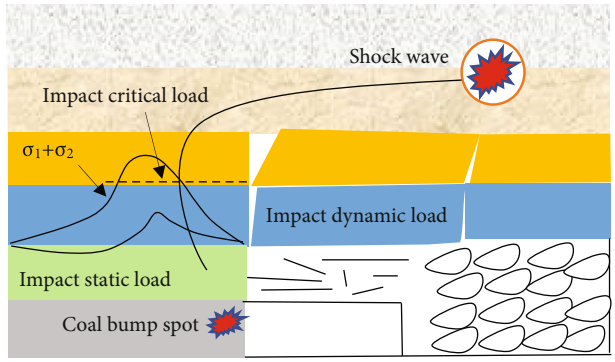

Figure 12: The coal bump model is due to the superposition of dynamic and static loads (σ_d and σ_s represent the static and dynamic stress, respectively, and $\sigma_d + \sigma_s$ represent the superposition of dynamic and static loads stress).

Table 2: Summary of peak intensity of 3 sets of coal samples.

Group	Paths	Peak intensity (MPa)	Average intensity (MPa)	Critical stress of coal bump (MPa)
1	1	17.26	15.26	15.7
	2	13.21		
	3	15.32		
2	1	12.45	14.02	
	2	17.39		
	3	12.24		
3	1	19.20	17.77	
	2	15.10		
	3	19.00		

on extensive research [22–24]. Classical coal bump mechanisms can be divided into two categories, one characterized by high static stress concentrations in the coal pillar and the other caused by dynamic stresses or shock waves due to rock movement at a considerable distance from the working face.

Different widths of coal pillars and working surfaces have significant effects on the sensitivity to vertical stress. The wider the coal pillar, the vertical stress decreases significantly. The wider the working face, the lower the vertical stress tends to be as the working face advances. Coal seams are subjected to certain static stresses due to gravity, tectonic stresses, and stresses caused by mining activities, while many factors cause shock waves during the mining process, such as hard top breaking, coal seam rupture, and blasting [25, 26]. These shock waves are transmitted to the perimeter of the mine or road and exert dynamic stresses on the coal or rock mass [27]. The total stress is an integration of static and dynamic stress, and the coal bump will certainly occur when the total stress exceeds the minimum critical value of coal bump.

4.2. Coal Bump Mechanism. Peak intensity is the mechanism of induced coal bump; different stress path is one of the factors affecting the occurrence of coal bump, both of which are the discriminatory criteria for induced rock bursts. Due to the influence of the internal structure of the coal samples, the peak intensity of the stress paths is significantly different. The mean value of peak intensity of the three groups lies within the 15.7 MPa. It can be shown that the higher the peak intensity, the greater the damage intensity, and when the average intensity range is exceeded, it will trigger the coal bump, as shown in Table 2.

The paper uses true triaxial experiments to study the destabilization of the coal rock system caused by coal sample damage, which is a high static load stress effect. Static energy concentration is a key factor causing coal bump; the higher the concentration of stress, the higher the probability of coal bump. In order to accurately describe this phenomenon, the study of the occurrence of coal bump mechanism can be described as follows:

$$\sigma_1 + \sigma_2 \geq \sigma_k, \tag{1}$$

where σ_1 represents the initial static stress of the coal body; σ_2 represents the dynamic stress caused by coal body damage; and σ_k represents the critical stress of coal bump.

From the true triaxial experiments, it is known that the critical stress σ_k coal bump is located in the 15.7 MPa; when the sum of the static stress and the dynamic stress caused by coal body damage is greater than 15.7 MPa, the coal rock system instability is triggered by coal bump.

5. On-Site Monitoring

5.1. Field Monitoring. Based on the characteristics of acoustic emission signals from the above experiments and the key monitoring areas obtained from numerical simulation

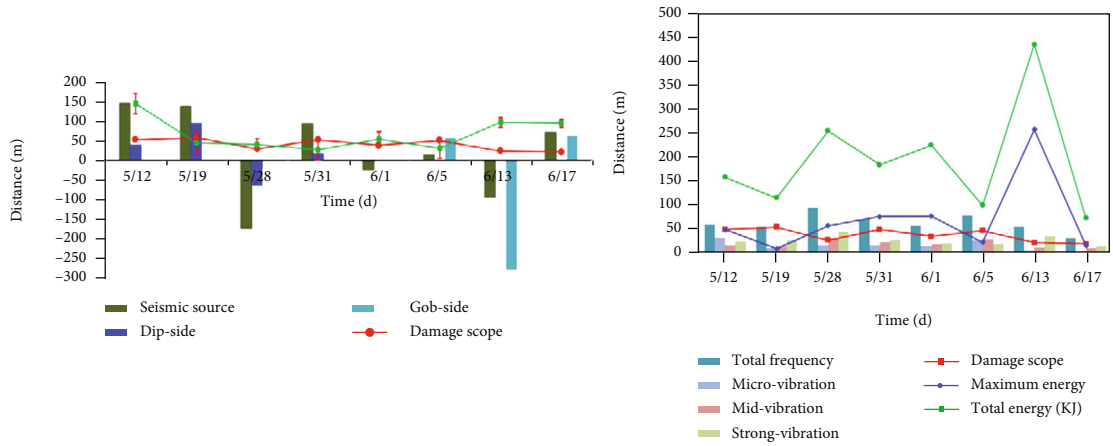

Figure 13: Rock burst event statistics.

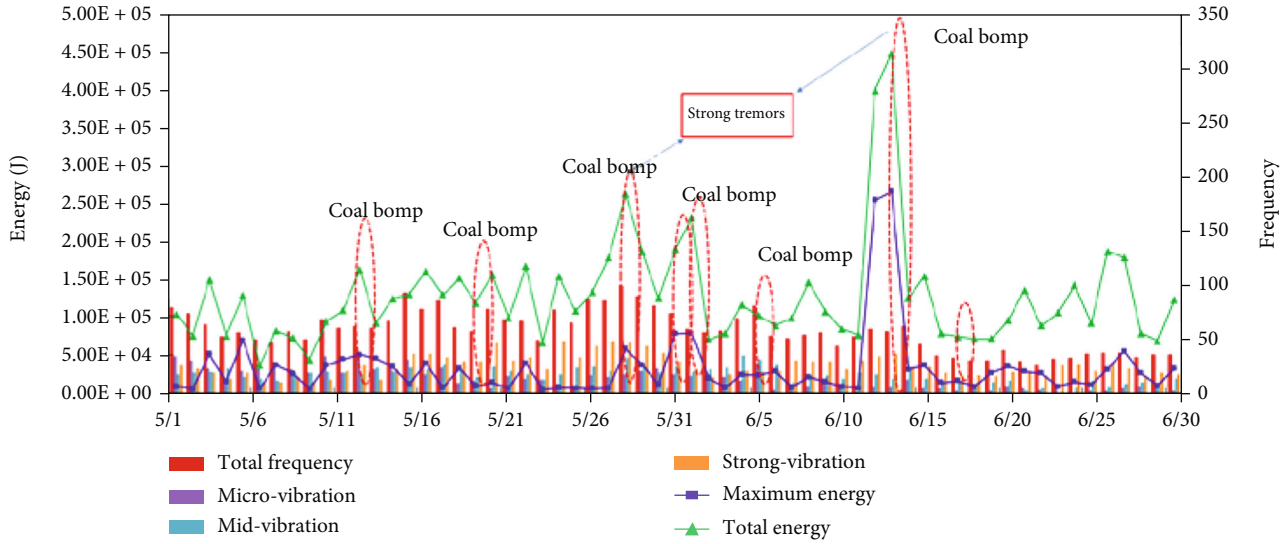

Figure 14: Time series of the tremors before the occurrence of rock bursts.

analysis, the electromagnetic emission (EME) method is used to reveal the microseismic law of coal bump occurring at the 401103 working face. The specific monitoring produce is shown below: three field recorder scones were placed at the mining face side along the ventilation roadway with an interval of 30~50 m; one field recorder scone was placed at the mining face side along the haulage roadway with an interval of 30 m to display the vibration of the surrounding rock of the mining face and roadway.

5.2. In-Site Energy Condition. During the mining process, the dynamic energy characterized by "coal bump" sound, local roadway caving and bottom drum, anchor (rope) off, and belt frame and rib spalling was frequently presented in the panel of #401103. Based on the electromagnetic emission (EME) monitoring system, the relationship between vibration energy and rock bursts frequency is investigated [28]. A total of 8 times coal bump occurred during the excavation of panel #401103, as shown in Figure 13 From May 12 to June 17, the microvibration, midvibration, strong vibration, damage scope, maximum energy, total energy, and the relationship between coal bump were observed. The maximum energy of 250 KJ ahead of the working face at 100 m and microvibration energy less than 50 KJ were obtained. The same phenomenon for midvibration and strong vibration occurred. A smoothing trend of damage scope was obtained. With the dynamic change of the damage scope, the location of coal bump also changed. The distance between the coal bump and the seismic source was approximately 50 m, as shown in Figure 13.

The coal bump mainly occurred at 100 m ahead of the mining face in the ventilation roadway. Vertical stress was mainly produced at the scope of 0~100 m ahead of the mining face associated with a 0~50 m damage region ahead of the mining face. At the same time, the frequent microvibration and midvibration can also lead to the occurrence of coal bump.

5.3. Response of the Mining Face. Figure 14 shows that the time series of the energy, vibration, and frequency were monitored by the EME system in the #401103 working face from May 1 to June 30. The total frequency showed slight fluctuation, indicating that the fracture did not get steady

in the coal body. The midvibration was activated, and at the same time, the accumulated energy was released inadequately, respectively; the energy concentration increased easily to the critical value and was released suddenly at one time, resulting in a serious rock bursts. The vibration activities during May 1 to June 30 demonstrated basically similar rules. From May 1 to June 30, the total energy almost remained at more than 2×10^5 J or less than 2×10^5 J. The coal bumps occurring on June 13 and 14 were characterized by a higher energy release, compared to the coal bumps occurring on May12, May 19, May 28, May 31, and June 1.

The total energy exhibited a "rise trend" during the 3 days, and occurrence probability of coal bump was high. After the coal bump, the EME and microvibration monitoring index remained at a relatively low level for several days, as the accumulated energy almost released, as shown in Figure 14.

In Figure 14, the frequency of tremors and total energy presented similar pattern to each other; as a result, there was no time for the energy to concentrate, and each impact was not enough to cause a catastrophe in the rock burst disaster. This provides a guide to the prevention of coal bump in high stress areas, facilitating the dissipation of energy in the control, and at the same time, this allows the effect of stress to be assessed.

Figure 14 describes the time series of the tremors before the occurrence of rock bursts. The microseismic signals were weak, and precursors were not obvious before the occurrence of the rock burst because the breakage of roof strata was prone to occur abruptly. The fracture of this stratum will cause strong dynamic stresses. As a result, the dynamic stresses generated by the fracture of the strata instantly feed high stresses into the coal and rock in the vicinity of the roadway, triggering rock bursts when the stresses reach the critical strength of the coal and rock [29]. The laws obtained from the field monitoring are well coupled with the basic experiments and numerical simulations.

6. Conclusions

(1) The acoustic emission shows signs of a sudden increase in stage when the coal sample appears to rupture. The increase in acoustic emission energy is not necessarily continuous

(2) Stress concentrations occur at the coal pillars and the gob in the range of 0~100 m in front of the working face, and there is a higher risk of coal bump in the roadway near the 401102 working face

(3) It is known that the critical stress σ_k coal bump is located in the 15.7 MPa; when the sum of the static stress and the dynamic stress caused by coal body damage is greater than 15.7 MPa, the coal rock system instability is triggered by coal bump

(4) The coal bump mainly occurred at 100 m ahead of the mining face in the ventilation roadway, the maximum energy up to 250 KJ

Data Availability

The data used to support the findings of this study are included within the article.

Conflicts of Interest

The authors declare no conflict of interest.

Acknowledgments

This work was supported by the Institute of Energy, Hefei Comprehensive National Science Center, under Grant No. 21KZS216; Postgraduate Innovation Fund, Anhui University of Science and Technology (2020CX2015); Open Fund of State Key Laboratory of Water Resource Protection and Utilization in Coal Mining (GJNY-18-73.7); National Youth Science Foundation (No. 51904011); Natural Science Foundation of Anhui Province (No. 1908085QE183); Anhui University Scientific Research Foundation (No. QN2018108); and Independent Research fund of the State Key Laboratory of Mining Response and Disaster Prevention and Control in Deep Coal Mines, Anhui University of Science and Technology (SKLMRDPC19ZZ05).

References

[1] H. Wang, B. A. Poulsen, B. Shen, S. Xue, and Y. Jiang, "The influence of roadway backfill on the coal pillar strength by numericalinvestigation," *International Journal of Rock Mechanics & Mining Sciences*, vol. 48, no. 3, pp. 443–450, 2011.

[2] K. Bo-Hyun, K. L. Mark, and H. E. Lawson, "Applying robust design to study the effects of stratigraphic characteristics on brittle failure and bump potential in a coal mine," in *36th Ground Control Conference*, 2017.

[3] B. María, D. Aguado, and C. González, "Influence of the stress state in a coal bump-prone deep coalbed: a case study," *International Journal of Rock Mechanics & Mining Sciences*, vol. 46, no. 2, pp. 333–345, 2009.

[4] X. Y. Li and Y. M. Li, "The instability mechanics of surrounding rock-coal mass system in longwall face and the prevention of pressure bumps," *Journal of Coal Science & Engineering (China)*, no. 1, pp. 47–50, 2003.

[5] S. Qin, "Instability leading to rock bursts and nonlinear evolutionary mechanisms for coal-pillar-and-roof system," *Journal of Engineering Geology*, vol. 13, no. 4, pp. 437–446, 2005.

[6] L. M. Dou, Z. L. Mu, Z. L. Li, A. Y. Cao, and S. Y. Gong, "Research progress of monitoring, forecasting, and prevention of rockburst in underground coal mining in China," *International Journal of Coal Science & Technology*, vol. 1, no. 3, pp. 278–288, 2014.

[7] M. D. G. Salamon, "Keynote address: some applications of geomechanical modeling and related research," in *Rock burst and Seismicity in Mines, Proceedings of the 3rd International Symposium*, pp. 279–309, Balkema, Rotterdam, 1993.

[8] P. K. Kaiser, "Observational modeling approach for design of underground excavations," in *Proceedings of International Workshop on Observational Method of Constructions of Large Underground Caverns in Difficult Ground Conditions*, pp. 1–7, Tokyo, 1995.

[9] C. A. Tang, *Catastrophe in Rock Unstable Failure (in Chinese)*, China Coal Industry Publishing House, Beijing, 1993.

[10] J. A. Wang and H. D. Park, "Comprehensive prediction of rockburst based on analysis of strain energy in rocks," *Tunnelling and Underground Space Technology*, vol. 16, no. 1, pp. 49–57, 2001.

[11] L. M. Dou, C. P. Lu, Z. L. Mu, and M. S. Gao, "Prevention and forecasting of rock burst hazards in coal mines," *Mining Science and Technology*, vol. 19, no. 5, pp. 585–591, 2009.

[12] R. Thom and Stabilite´ Structurelle, *Morphoge'ne'se*, Benjamin, New York, 1972.

[13] S. Henley, "Catastrophe theory models in geology," *Journal of the International Association for Mathematical Geology*, vol. 8, no. 6, pp. 649–655, 1976.

[14] Y. S. Pan and M. T. Zhang, "Analysis on the physical process of rock bursts by catastrophe theory (in Chinese)," *Jiang Fuxin Mining Institution*, vol. 11, no. 1, pp. 12–18, 1992.

[15] S. Q. Qin, Z. Y. Zhang, and S. T. Wang, *An Introduction to Nonlinear Engineering Geology*, Southwest University Press of Transportation, Chengdu, PR China, 1993.

[16] Z. H. Xu, X. H. Xu, and C. A. Tang, "Analysis of a cusp catastrophe bump of coal pillar under hard rocks," *Journal China Coal Society*, vol. 20, no. 5, pp. 191–485, 1995.

[17] P. K. Kaiser and C. A. Tang, "Numerical simulation of damage accumulation and seismic energy release during brittle rock failure–part II: rib pillar collapse," *International Journal of Rock Mechanics & Mining Sciences & Geomechanics Abstracts*, vol. 35, no. 2, pp. 123–134, 1998.

[18] C. P. Lu and L. M. Dou, "The relationship between vertical stress gradient, seismic, and electromagnetic emission signals at Sanhejian coal mine, China," *International Journal of Rock Mechanics & Mining Sciences*, vol. 70, pp. 90–100, 2014.

[19] P. K. Kaiser, D. D. Tannant, and D. R. McCreath, "Support of tunnels in burst-prone ground," in *Proceedings of 8th International Congress on Rock Mechanisms*, vol. 2, pp. 471–477, Tokyo, 1995.

[20] Y. Xue, J. Liu, P. G. Ranjith, Z. Zhang, F. Gao, and S. Wang, "Experimental investigation on the nonlinear characteristics of energy evolution and failure characteristics of coal under different gas pressures," *Bulletin of Engineering Geology and the Environment*, vol. 81, no. 1, p. 38, 2022.

[21] P. Hou, Y. Xue, F. Gao et al., "Effect of liquid nitrogen cooling on mechanical characteristics and fracture morphology of layer coal under Brazilian splitting test," *International Journal of Rock Mechanics and Mining Sciences*, vol. 151, article 105026, 2022.

[22] Y. S. Yang, S. J. Wei, and D. M. Zhang, "Influence of rock burst and other disasters on stability of surrounding rock of roadway," *Geotechnical and Geological Engineering*, vol. 36, no. 3, pp. 1767–1777, 2018.

[23] H. W. Zhang, E. Derek, and Z. J. Wan, "Failure response of composite rock-coal samples," *Geomechanics and Geophysics for Geo-Energy and Geo-Resources*, vol. 4, no. 2, pp. 175–192, 2018.

[24] Y. Y. Pu, A. Derek, and H. W. Xu, "A principal component analysis/fuzzy comprehensive evaluation for rockburst potential in kimberlite," *Pure and Applied Geophysics*, vol. 175, no. 6, pp. 2141–2151, 2018.

[25] X. J. Hao, W. S. Du, and Y. X. Zhao, "Dynamic tensile behaviour and crack propagation of coal under coupled static-dynamic loading," *International Journal of Mining Science and Technology*, vol. 30, no. 5, pp. 659–668, 2020.

[26] X. J. Hao, Y. N. Wei, and K. Yang, "Anisotropy of crack initiation strength and damage strength of coal reservoirs," *Petroleum Exploration and Development*, vol. 48, no. 1, pp. 243–255, 2021.

[27] J. F. Lou, F. Q. Gao, J. H. Yang et al., "Characteristics of evolution of mining-induced stress field in the longwall panel: insights from physical modeling," *International Journal of Coal Science and Technology*, vol. 8, no. 5, pp. 938–955, 2021.

[28] H. Hu, D. Ldc, and D. Sgb, "Microseismic and electromagnetic coupling method for coal bump risk assessment based on dynamic static energy principles," *Safety Science*, vol. 114, pp. 30–39, 2019.

[29] G. Wang, S. Gong, L. Dou, W. Cai, X. Yuan, and C. Fan, "Rockburst mechanism and control in coal seam with both syncline and hard strata," *Safety Science*, vol. 115, pp. 320–328, 2019.